materials

MDI

Article

Effect of Oxygen Nonstoichiometry on Electrical Conductivity and Thermopower of $Gd_{0.2}Sr_{0.8}FeO_{3-\delta}$ Ferrite Samples

Vyacheslav Dudnikov [1], Yury Orlov [1], Aleksandr Fedorov [1,2,*], Leonid Solovyov [3], Sergey Vereshchagin [3], Alexander Burkov [4], Sergey Novikov [3], and Sergey Ovchinnikov [1,2]

[1] Kirensky Institute of Physics, Federal Research Center KSC Siberian Branch Russian Academy of Sciences, Krasnoyarsk, 660036 Russia

[2] Institute of Engineering Physics and Radio Electronics, Siberian Federal University, Krasnoyarsk, 660041 Russia

[3] Institute of Chemistry and Chemical Technology, Federal Research Center KSC Siberian Branch Russian Academy of Sciences, Krasnoyarsk, 660036 Russia

[4] Ioffe Institute, St. Petersburg, 194021 Russia

***** Correspondence: alex99@iph.krasn.ru; Tel.: +7904-898-5175

Received: 27 November 2018; Accepted: 21 December 2018; Published: date

Abstract: The behavior of the resistivity and thermopower of the $Gd_{0.2}Sr_{0.8}FeO_{3-\delta}$ ferrite samples with a perovskite structure and the sample stability in an inert gas atmosphere in the temperature range of 300–800 K have been examined. It has been established that, in the investigated temperature range, the thermoelectric properties in the heating–cooling mode are stabilized at $\delta \geq 0.21$. It is shown that the temperature dependencies of the resistivity obtained at different δ values obey the activation law up to the temperatures corresponding to the intense oxygen removal from a sample. The semiconductor–semiconductor electronic transitions accompanied by a decrease in the activation energy have been observed with increasing temperature. The maximum thermoelectric power factor of 0.1 μW/(cm K2) was found for oxygen nonstoichiometric sample at T = 800 K.

Keywords: rare-earth-substituted cobalt oxides; stability; thermoelectric properties

1. Introduction

The major characteristics of a thermoelectric material are its thermoelectric efficiency $Z = S^2\sigma/\varkappa$ (S is the Seebeck coefficient, also known as thermopower, σ is the electrical conductivity, and $\varkappa$ is the thermal conductivity) [1], dimensionless thermoelectric quality factor ZT (T is the absolute temperature), and power factor $P = S^2\sigma = S^2/\rho$ (ϱ is the resistivity).

Recently, close attention of researchers has been paid to oxide materials [2], since they are stable against high temperatures, nontoxic, and, as a rule, do not contain rare elements. A group of complex oxides of the rare-earth transition metals $Ln_{1-x}A_xMO_{3-\delta}$ (Ln is a lanthanoid, A is an alkali or alkali-earth metal, and M is a transition metal (Co, Fe, or Mn)) with a perovskite structure is holding a special place [3–5] among the oxides for promising application. The diverse physicochemical properties of these compounds, which belong to strongly correlated electron systems, are interesting both for application [6] and for fundamental research. Along with their thermoelectric characteristics, the stability of these materials against different environmental factors, including the atmospheric composition and temperature, is of great practical importance. In this study, taking into account the significant differences between the low-temperature properties of the $Gd_{1-x}Sr_xFeO_{3-\delta}$ compounds with different oxygen nonstoichiometry indices δ [7] and the high mobility of oxygen in the $Gd_{1-x}Sr_xCoO_{3-\delta}$ compounds [8], we investigate the effect of the oxygen nonstoichiometry on the thermoelectric properties of the $Gd_{0.2}Sr_{0.8}FeO_{3-\delta}$ compound and its stability in the temperature range of 300–800 K.

2. Materials and Methods

Sample synthesis. The $Gd_{0.2}Sr_{0.8}FeO_{3-\delta}$ samples were obtained using the glycinenitrate-based solution-combustion synthesis [9]. The initial components of the perovskiteoxide were cations of nitrates of each metal component ($Gd(NO_3)_3 \cdot 6H_2O$, 99.9% trace metal basis, Rare Metals Plant, Novosibirsk, Russia; $Sr(NO_3)_2$, >99.0%, Reachim, Moscow, Russia; $Fe(NO_3)_3 \cdot 9H_2O$, >98%, Sigma-Aldrich). The initial gel was obtained via evaporation of the glycinenitrate-based solution at 363 K with subsequent heating until combustion at a low rate. The prepared powder was calcinated in air at 723 K for 5 h, thoroughly grinded in an agate mortar, and sintered in air at 1623 K for 5 h with subsequent cooling to room temperature at a rate of 2 °C/min. Tablets were synthesized at T_c = 1473 K for 24 h and cooled in the same mode.

The oxygen nonstoichiometry of the samples was determined using a NETZSCHSTA449C analyzer equipped with an Aëolos QMS 403C mass spectrometer (NETZSCH, Selb, Germany). The measurements were performed in the 5% H_2-Ar mixture flow in a corundum crucible with a perforated cover. The sample mass was 30 mg. The oxygen content in the $Gd_{0.2}Sr_{0.8}FeO_{3-\delta}$samples was determined from the mass decrement Δm using the equation $\delta(T) = \delta_0 + M\Delta m(T)/1600$, where $\delta(T)$ is the δ value at temperature T, $\Delta m(T)$ (%) is the mass decrement at this temperature, and M is the molecular mass of the $Gd_{0.2}Sr_{0.8}FeO_{2.87}$ compound. The measurement error was δ = ±0.01. The oxygen nonstoichiometry index of the initial $Sr_{0.8}Gd_{0.2}FeO_{3-\delta}$ material was taken to be δ_0 = 0.13, according to the data on the Gd-Sr-Fe perovskite synthesized using the same technique [7].

The X-ray diffraction measurements were performed on powder diffractometer (PANalytical X'Pert PRO, Netherlands) using Cu $K\alpha$ radiation in the 2θ-angular

range of 20–158°. The crystal structure was refined using the derivative difference minimization (DDM) method [10]. Temperature dependences of the thermopower and resistivity were obtained on an experimental setup developed at the Ioffe Institute, St. Petersburg [11,12].

3. Results

In contrast to the complex cobalt oxides $Re_{1-x}Sr_xCoO_{3-\delta}$ (Re is the rare-earth ion), which, depending on the cooling rate and synthesis temperature, can form compounds ordered or disordered over A sites of the perovskite structure [13–18], the $Gd_{0.2}Sr_{0.8}FeO_{3-\delta}$ compound synthesized by us is disordered and characterized by the random distribution of oxygen vacancies and cations over the A sites. The X-ray diffraction study revealed no foreign phases. According to the X-ray powder diffraction (XRD) data (Figure 1), the synthesized $Gd_{0.2}Sr_{0.8}FeO_{3-\delta}$ samples, similar to the heavily-doped $La_{1-x}Sr_xFeO_{3-\delta}$ ($0.8 \le x \le 1.0$) compounds [19], have a form of a disordered perovskite with the cubic symmetry (sp. gr.Pm3m (a = 3.8688(1) Å), in which all the iron sites were identical, as in the mixed-valence iron compounds $Sr_2LaFe_3O_{8.94}$ [20]. The structural formula derived from the refined occupancies of atomic positions (Table 1) was $Sr_{0.8}Gd_{0.2}FeO_{2.79}$. Similar perovskites $Sr_{0.75}Gd_{0.25}FeO_{2.87}$ and $Sr_{0.75}Gd_{0.25}FeO_{2.94}$ described in [7] have smaller lattice parameters (3.8665(1) and 3.8582(1) Å), which is consistent with the smaller oxygen stoichiometry estimated from the XRD refinement for our sample.

Atomic positions, and their occupancies and thermal parameters in the crystal structure of $Sr_{0.8}Gd_{0.2}FeO_{2.79}$ are given in Table 1.

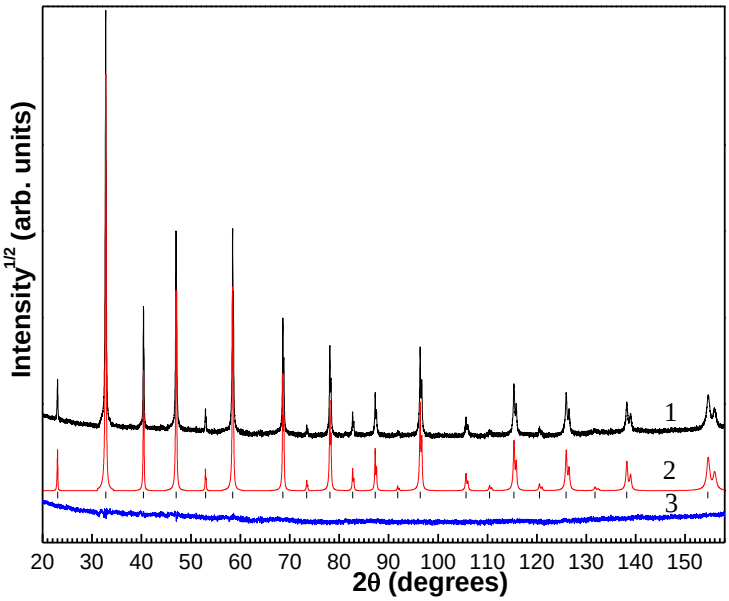

Figure 1. Experimental (1), calculated (2), and difference (3) X-ray diffraction patterns of the $Gd_{0.2}Sr_{0.8}FeO_{2.79}$ compound after DDM refinement.

Table 1. Atomic positions, and their occupancies and thermal parameters in the crystal structure of $Sr_{0.8}Gd_{0.2}FeO_{2.79}$. Space group is Pm3m, with lattice parameter a = 3.8688(1) Å.

Atom	Position	Occupancy	x	y	z	U_{iso} [Å^2]
Sr	1a	0.800(4)	0	0	0	0.0092(7)
Gd	6e	0.0334(7)	0.080(4)	0	0	0.0092(7)
Fe	1b	1	1/2	1/2	1/2	0.0082(5)
O	12h	0.232(1)	0.452(2)	1/2	0	0.0211(14)

Figure 2 shows the temperature-programmed reduction data. The change in the mass caused by removal of oxygen from the sample upon heating in the 5%H_2-Ar reducing atmosphere started at ≈500 K and depended on the heating rate, which is related to the solid-state reduction kinetics. As the heating rate increased, the thermogravimetric (TG) and derivative thermogravimetric (DTG) curves shifted to the high-temperature region and the maximum reduction rate was observed at 640 and 725 K at heating rates of 2 and 20 K/min, respectively.

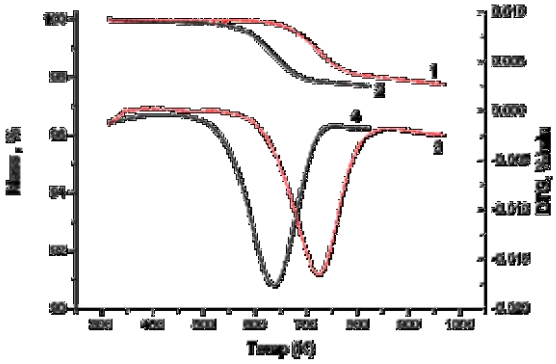

Figure 2. (1, 2) TG and (3, 4) DTG curves of temperature-programmed reduction of the $Gd_{0.2}Sr_{0.8}FeO_{2.87}$ compound in the 5% H_2-Ar mixture flow at heating rates of 2 (black solid curve) and 20 K/min (red dotted curve).

The electrical resistivity and thermopower were measured on the rectangular bar samples 0.9 × 4.5 × 9 mm in size at temperatures from 300 to 800 K in the inert He (99.999%) atmosphere. To examine the changes in the temperature dependences of the resistivity and thermopower, the measurements were performed during the heating–cooling cycles. Three thermal cycles were performed. The heating and cooling rates were 5 °C/min. The results obtained are shown in Figure 3. It can be seen that the temperature dependences of the electrical resistivity and thermopower of the investigated samples in the heating–cooling cycles were essentially different, which is indicative of the strong effect of oxygen on the physical properties of the $Gd_{0.2}Sr_{0.8}FeO_{3-\delta}$ compound. In the first thermocycle, when oxygen was actively removed from the sample, the behavior of the thermoelectric parameters of the compound was especially anomalous (Figure

4a). For clarity, the electrical resistivity and Seebeck coefficient measured during the first heating with the active oxygen removal (Figure 4a) and the last cooling (Figure 4b), when the sample was almost stable, are plotted.

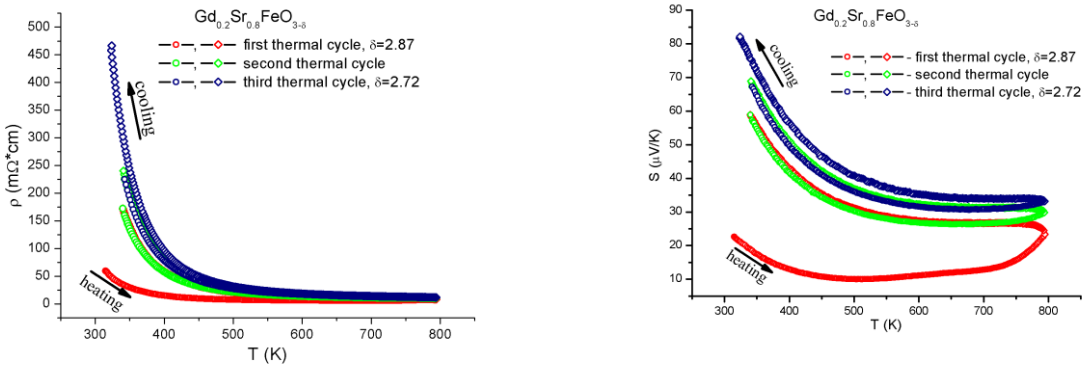

Figure 3. Temperature dependences of (a) the resistivity and (b) thermopower for three sequential heating–cooling cycles.

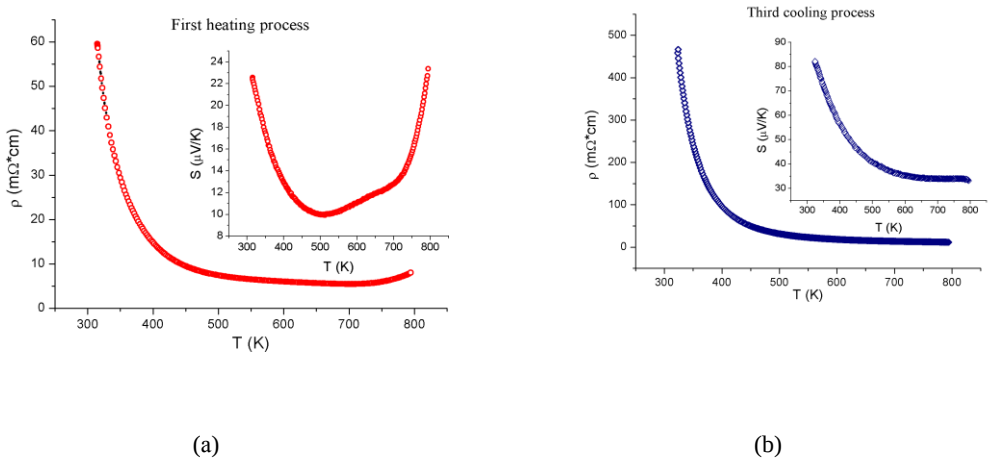

Figure 4. Temperature dependences of the resistivity and thermopower (insets) during (**a**) the first heating and (**b**) the third cooling.

The anomalies in the behavior of the electrical resistivity and Seebeck coefficient correlated with the data of thermogravimetric analysis of the sample mass loss caused by the removal of oxygen (Figure 4a).

The oxygen nonstoichiometry index δ increased from one heating–cooling cycle to another and the deviation from the semiconductor-type conductivity shifted toward higher temperatures. At δ = 0.21, the temperature dependency of the resistivity was qualitatively consistent with the semiconductor-type conductivity dρ/dT< 0 over the entire temperature range of interest (Figure 4b). The conductivity in the regions corresponding to the semiconductor type obeyed the thermal activation law:

$$\rho(T) = \rho_0 \times exp\ (E_a/k_B T) \quad (1)$$

where ρ_0 is the coefficient weakly dependent on temperature, E_a is the activation energy, and k_B is the Boltzmann constant. The dependences of the logarithmic resistivity of the sample on the reciprocal temperature in the corresponding temperature ranges for several heating and cooling processes are presented in Figure 5. For all the thermal cycles, the ln(ϱ)(1/T) curves contain two regions that are described well by the thermal activation law with different activation energies E_a. At each specific δ value, the activation energy decreased with increasing temperature. At the same time, the activation energy grew with the oxygen nonstoichiometric index.

The absolute values of the oxygen nonstoichiometry indices, the activation energies for different temperature ranges, and the electronic transition temperatures, determined by the crossing points of the approximation curves (Figure 5), are given in Table 2.

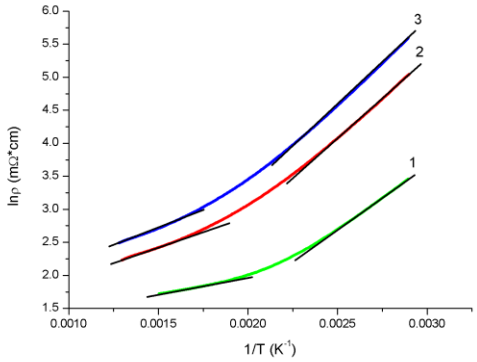

Figure 5. Reciprocal temperature dependence of the $Gd_{0.2}Sr_{0.8}FeO_{3-\delta}$ logarithmic resistivity. Black straight lines show the thermal activation law processing: (1) first heating, (2) first cooling, and (3) third cooling.

Figure 6 presents the plots of activation energy E_a in the low-temperature (below the temperature of the electronic transition, $T < T_{p\text{-}p}$) and high-temperature (above the transition temperature, $T > T_{p\text{-}p}$) regions and semiconductor–semiconductor transition temperature $T_{p\text{-}p}$ as functions of the oxygen content in the sample. It can be seen that, in the investigated temperature and δ ranges, all the dependencies are linear.

Table 2. Oxygen nonstoichiometry indices, activation energies, and electronic transition temperatures for the $Gd_{0.2}Sr_{0.8}FeO_{3-\delta}$ ferrite sample.

Regime	δ	E_a ($T < T_{p\text{-}p}$) (eV)	$T_{p\text{-}p}$ (K)	E_a ($T > T_{p\text{-}p}$) (eV)
First heating	0.13 ± 0.01	0.16 ± 0.01	461 ± 1	0.04 ± 0.01
First cooling	0.19 ± 0.01	0.20 ± 0.01	495 ± 1	0.07 ± 0.01

Second cooling	0.20 ± 0.01	0.21 ± 0.01	502 ± 1	0.08 ± 0.01
Third cooling	0.21 ± 0.01	0.22 ± 0.01	507 ± 1	0.09 ± 0.01

The E_a value in the low-temperature range is several times higher than in the high-temperature range; the difference slightly decreased with increasing δ. The charge carrier concentration, necessary for the observed electrical conductivity, is induced by different-valence Gd+3/Sr+2 cation substitutions and holes related to oxygen vacancies. At high temperatures, we observed the properties of an almost degenerate semiconductor, while at low temperatures, the activation energy increased. The temperature $T_{p\text{-}p}$ of the asymptotic change is weakly depended on the vacancy concentration. The fact that the activation energy depends on the vacancy concentration indicates, that the impurity level shifts away from the band extremum. It is worth noting that the concentration dependences of the activation energies (straights 1 and 2 in Figure 6) are almost parallel.

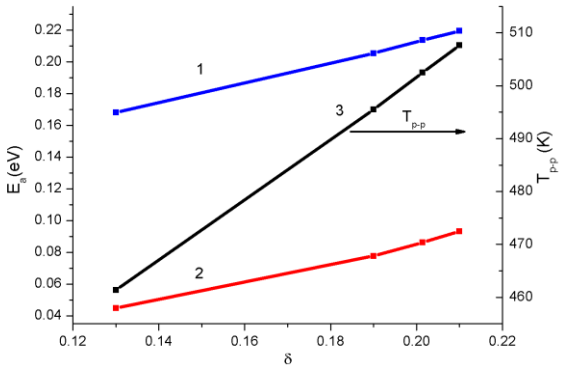

Figure 6. Dependencies of the activation energy E_a: (1) is the temperature region below the electronic transition and (2) is the high-temperature region, and (3) semiconductor–semiconductor transition temperature $T_{p\text{-}p}$ on the oxygen nonstoichiometry index.

Figure 7 shows the temperature dependencies of the power factor P for the first and last temperature cycles. It can be seen that, as the temperature increased, the power factor of the samples grew, but did not attain its maximum, in the investigated temperature range. In the sample stability region, the increase was monotonic, without jumps, and almost linear for the sample with δ = 0.21. At a temperature of T = 500 K, the power factor of the sample with δ = 0.21 exceeded almost fourfold the power factor of the samples with δ = 0.13 (0.052 μW/(K²cm) and 0.013 μW/(K²cm)) and the maximum P value obtained at T = 800 K was 0.1 μW/(K²cm).

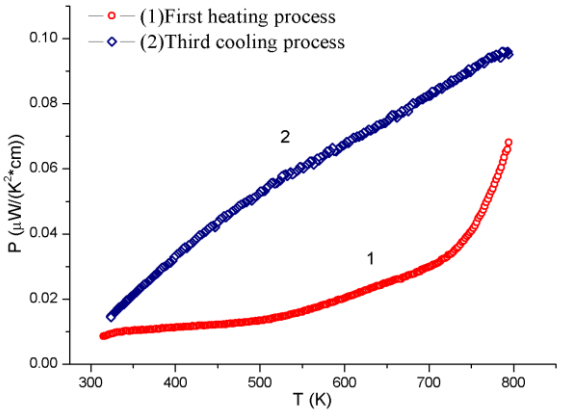

Figure 7. Temperature dependences of the power factor P for the first heating (δ = 0.13 at T = 300 K) (1) and the third cooling (δ = 0.21) (2).

The power factors obtained in this work for the sample $Gd_{0.2}Sr_{0.8}FeO_{3-\delta}$ (P = 0.1 μW/(cm·K²)) are consistent with those presented in Reference [21] for the $LaCo_{1-x}Ni_xO_3$ (P = 0,12 μW/(cm·K²), $LaCo_{1-x}Ti_xO_{3-\delta}$ (P = 0.28 μW/(cm·K²)) [22], $La_{1-x}Sr_xCo_{0.8}Ni_{0.1}Fe_{0.1}O_3$ (P = 0.76 μW/(cm·K²)) [5], and $La_{1-x}Na_xCoO_3$ (P = 0.1μW/(cm·K²)) polycrystalline samples [23], although our data are inferior to the value of P ≈ 3 μW/(cm·K²) for the $Ca_{3-x}Bi_xCo_4O_{9+\delta}$ samples from study [24].

5. Conclusions

The behavior of electrical resistivity and thermopower of the disordered $Gd_{0.2}Sr_{0.8}FeO_{3-\delta}$ perovskite in the temperature range of 300–800 K and its stability in the helium atmosphere were investigated. It was established that the stability of thermoelectric parameters strongly depends on the oxygen content in a sample. The samples with the oxygen nonstoichiometric index δ of 0.21 or larger are stable at temperatures from 300 to 800 K. In the sample stability region, the temperature dependences of electrical resistivity for all δ values contained portions that are well described by the thermal activation law. At elevated temperatures we observe a semiconductor-semiconductor transition, which is accompanied by a decrease of the activation energy. The activation energy and the temperature of the transition increase with increasing oxygen nonstoichiometry.

We explained the nature of the semiconductor transitions as the result of occupancy/ deoccupancy by the oxygen ions of different positions in the nonstoichiometry lattice. The electron bands near the Fermi level substantially changed and led to significant changes in the band gap and the activation energy. The activation energies in the low- and high-temperature regions depended similarly on the δ value. The increase in the δ value led to the significant enhancement of the power factor *P*. In particular, at a temperature of *T* = 500 K, the power factor of the sample with δ = 0.21 was almost fourfold higher than the power factor of the samples with δ = 0.13 (0.052 μW/(K²cm) and 0.013 μW/(K²cm). In the sample with δ = 0.21, the power factor increased with temperature almost

linearly and attained its maximum value of 0.1 μW/(cm·K^2) at T = 800 K. Thus, varying the oxygen content in a sample, one can control the temperature ranges of stability and the power factor of the complex transition metal oxides.

Author Contributions: Conceptualization & Methodology, Vyacheslav Dudnikov and Sergey Ovchinnikov; Investigation, Alexander Burkov, Sergey Vereshchagin, Leonid Solovyov and Sergey Novikov; Writing-Original Draft Preparation, Yury Orlov; Writing-Review & Editing, Aleksandr Fedorov.; Visualization, Vyacheslav Dudnikov.; Supervision, Project Administration & Funding Acquisition, Aleksandr Fedorov.

Funding: This research was funded by the Russian Science Foundation, project no. 16-13-00060.

Conflicts of Interest: The authors declare no conflict of interest.

References

1. Ioffe, A.F. *Semiconductor Thermoelements, and Thermoelectric Cooling (Infosearch, London 1957)*; Rowe, D.M., Ed.; CRC Handbook of Thermoelectrics; CRC Press, 1995.
2. Shiand, X.; Chenand, L.; Uher, C. Recent advances in high-performance bulk thermoelectric materials. *Int. Mater. Rev.* **2016**, *61*, 379–415.
3. Terasaki, I.; Sasago, Y.; Uchinokura, K. Large thermoelectric power in $NaCo_2O_4$ single crystals. *Phys. Rev. B* **1997**, *56*, R12685, doi:10.1103/PhysRevB.56.R12685.
4. Weidenkaff, A.; Aguirre, M.H.; Bocher, L.; Trottmann, M.; Tomes, P.; Robert, R. Development of Perovskite-type Cobaltates and Manganates for Thermoelectric Oxide Modules. *J. Korean Ceram. Soc.* **2010**, *47*, 47–53, doi:10.4191/KCERS.2010.47.1.047.
5. Harizanova, S.G.; Zhecheva, E.N.; Valchev, V.D.; Khristova, M.G.; Stoyanova, R.K. Improving the thermoelectric efficiency of Co based ceramics. *Mater. Today Proc.* **2015**, *2*, 4256–4261, doi:10.1016/j.matpr.2015.09.011.
6. Zlatić, V.; Boyd, G.R.; Freericks, J.K. Universal thermopower of bad metals. *Phys. Rev. B* **2014**, *89*, 155101.
7. Blasco, J.; Stankiewicz, J.; García, J. Phase segregation in the $Gd_{1-x}Sr_xFeO_{3-\delta}$ series. *J. Solid State Chem.* **2006**, *179*, 898–908, doi:10.1016/j.jssc.2005.12.023.
8. Vereshchagin, S.N.; Dudnikov, V.A.; Solovyov, L.A. Study of Mobile Oxygen in Ordered/Disordered Nonstoichiometric Sr-Gd-Cobaltate by Simultaneous Thermal Analysis. *J. Sib. Fed. Univ. Chem.* **2017**, *10*, 346–357, doi:10.17516/1998-2836-0031.
9. Chick, L.A.; Pederson, L.R.; Maupin, G.D.; Bates, J.L.; Thomas, L.E.; Exarhos, G. J., Glycine-nitrate combustion synthesis of oxide ceramic powders, Materials Letters 1990, 10, 6.
10. Solovyov, L. A. Full-Profile Refinement by Derivative Difference Minimization. *J. Appl. Crystallogr.* **2004**, *37*, 743−749.
11. Burkov, A.T.; A Heinrich, P P Konstantinov, T Nakama and K Yagasaki, Experimental set-up for thermopower and resistivity measurements at 100–1300 K; Measurement Science and Technology, 2001, 12, 264–272.
12. Burkov, A.T.; Fedotov, A.I.; Kasyanov, A.A.; Panteleev, R.I.; Nakama, T. Methods and technique of thermopower and electricalconductivity measurements of thermoelectric materials at high temperatures. *Sci. Tech. J. Inf. Technol. Mech. Opt.* **2015**, *15*, 173–195, doi:10.17586/2226-1494-2015-15-2-173-195.
13. James, M.; Tedesco, T.; Cassidy, D.J.; Withers, R.L., Oxygen vacancy ordering in strontium doped rare earth cobaltate perovskites Ln1−xSrxCoO3−δ (Ln=La, Pr and Nd; x>0.60), Materials Research Bulletin, 2005, 40, 990.
14. James, M.; Morales, L.; Wallwork, K., Structure and Magnetism in Rare Eath Strontium-Doped Cobaltates, Physica B, 2006, 199, 385–386.
15. Vereshchagin, S.N.; Dudnikov, V.A.; Shishkina, N.N.; Solovyov, L.A. Phase transformation behavior of $Sr_{0.8}Gd_{0.2}CoO_{3-\delta}$perovskite in the vicinity of order-disorder transition. *Thermochim. Acta* **2017**, *655*, 34–41, doi:10.1016/j.tca.2017.06.003.
16. Vereshchagin, S.N.; Solovyov, L.A.; Rabchevskii, E.V.; Dudnikov, V.A.; Ovchinnikov, S.G.; Anshits, A.G. Methane oxidation over A-site ordered and disordered $Sr_{0.8}Gd_{0.2}CoO_{3-d}$perovskites. *Chem. Commun.* **2014**, *50*, 6112–6115.
17. Yoshida, Kobayashi, W.; Nakano, T.; Terasaki, I.; Matsubayashi, K.; Uwatoko, Y.; Grigoraviciute, I.; Karppinen, M.; Yamauchi, H. Chemical and physical pressure effects on the magnetic and transport

properties of the A-site ordered perovskite $Sr_3YCo_4O_{10.5}$. *J. Phys. Soc. Jpn.* **2009**, *78*, 094711, doi:10.1143/JPSJ.78.094711.

18. Fukushima, S.; Sato, T.; Akahoshi, D.; Kuwahara, H. Comparative study of ordered and disordered $Y_{1-x}Sr_xCoO_{3-\delta}$. *J. Appl. Phys.* **2008**, *103*, 07F705, doi:10.1063/1.2830615.
19. Dann, S.E.; Currie, D.B.; Weller, M.T.; Thomas, M.F.; Al-Rawwas, A.D. The Effect of Oxygen Stoichiometry on Phase Relations and Structure in the System $La_{1-x}Sr_xFeO_{3-\delta}$ (0 <= x <= 1, 0 <= δ<= 0.5). *J. Solid State Chem.* **1994**, *109*, 134–144, doi:10.1006/jssc.1994.1083.
20. Battle, P.D.; Gibb, T.C.; Lightfoot, P. The structural consequences of charge disproportionation in mixed-valence iron oxides. The crystal structure of $Sr_2LaFe_3O_{8.94}$ at room temperature and 50 K. *J. Solid State Chem*. **1990**, *84*, 271–279, doi:10.1016/0022-4596(90)90325-R.
21. Robert, R.; Aguirre, M.H.; Bocher, L.; Trottmann, M.; Heiroth, S.; Lippert, T.; Döbeli, M.; Weidenkaff, A. Thermoelectric Properties of $LaCo_{1-x}NixO_3$ Polycrystalline Samples and Epitaxial Thin Films. *Solid State Sci.* **2008**, *10*, 502–507.
22. Robert, R.; Bocher, L.; Trottmann, M.; Reller, A.; Weidenkaff, A. Synthesis and High-Temperature Thermoelectric Properties of Ni and Ti Substituted $LaCoO_3$. *J. Solid State Chem.* **2006**, *179*, 3893–3899.
23. Behera, S.; Kamble, V.B.; Vitta, S.; Umarji, A.M.; Shivakumara, C. Synthesis Structure and Thermoelectric Properties of La1-xNaxCoO3 Perovskite Oxides. *Bull. Mater. Sci.* **2017**, *40*, 1291–1299.
24. Moser, D.; Karvonen, L.; Populoh, S.; Trottmann, M.; Weidenkaff, A. Influence of the Oxygen Content on Thermoelectric Properties of $Ca_{3-x}BixCo_4O_{9+\delta}$ System. *Solid State Sci.* **2011**, *13*, 2160–2164.